Journal of Crystal Growth 412 (2015) 87–94

Contents lists available at ScienceDirect

Journal of Crystal Growth

journal homepage: www.elsevier.com/locate/jcrysgro

Growth and kinetic Monte Carlo simulation of InAs quantum wires on vicinal substrates

Andrew Scullion [a], David A. Thompson [b], Gianluigi A. Botton [a,*]

[a] Department of Materials Science and Engineering, McMaster University, 1280, Main St. W, Hamilton, Ontario, Canada L8S 4L7
[b] Centre for Emerging Devices and Technology, McMaster University, 1280, Main St. W, Hamilton, Ontario, Canada L8S 4L7

ARTICLE INFO

Article history:
Received 5 September 2014
Received in revised form
16 November 2014
Accepted 17 November 2014
Communicated by K. Deppert
Available online 25 November 2014

Keywords:
A1. Computer simulation
A1. Nanostructures
A1. Electron microscopy
A1. Nucleation
A3. Molecular beam epitaxy
B2. Semiconducting III–V materials

ABSTRACT

Self-assembled quantum structures have been successfully grown for some time now but control over their uniformity has proven difficult due to the stochastic nature of surface diffusion. We have investigated the effect of vicinal InP(001) substrates on the uniformity of InAs quantum wires grown on InGaAlAs lattice-matched to InP using molecular beam epitaxy. Dense quantum wires were grown on both nominally flat and vicinal substrates off-cut by 0.9° toward the [110] direction for comparison. The off-cut angle was chosen to provide terraces which match the orientation and spacing of wires grown on nominally flat substrates. A modest but statistically significant improvement in the size distribution of the wires was observed on vicinal substrates through the analysis of ultrahigh resolution scanning electron micrographs. The interface between the wires and the off-cut substrate was studied using cross-sectional high resolution scanning transmission electron microscopy. In addition, a kinetic Monte Carlo model of epitaxial growth including full strain calculations was developed to further investigate the nucleation process. Using an anisotropic bond model to account for the surface energy of different crystallographic facets, our simulations produced wires similar to those observed experimentally while demonstrating the importance of anisotropic bonding compared to anisotropic diffusion. Growth on vicinal substrates is also simulated here and indicates that off-cut substrates should indeed improve the size distribution of quantum wires under proper growth conditions.

1. Introduction

Compared to two-dimensional quantum well heterostructures used in light emitting devices (such as solid state lasers), quantum wires have the potential of reducing the linewidth of their luminescence spectrum through its narrower density of states. A narrow spectrum is important for a high bandwidth in telecommunication applications and for the gain of laser devices [1]. Moreover, self-assembled quantum wire lasers exhibit a lower threshold current density and are less sensitive to temperature which is important in many applications [2]. Infrared lasers with a wavelength around 1.55 μm, which corresponds to a minimum in the absorption spectrum of SiO_2 [3], have been successfully produced [4,5] but their photoluminescence spectra remain broad due to the broad size distribution of the wires. This could potentially be solved by patterning substrates but the process is expensive and time consuming. On the other hand, InAs quantum dot lasers on GaAs have been thoroughly investigated [6,1] and there has been much progress in terms of producing homogeneous dots but their spectral output is around 1.3 μm. Moreover, controlling their uniformity seems to be at the expense of density [1,7].

InAs quantum wires grown by molecular beam epitaxy (MBE) on InGaAlAs lattice-matched to InP have been shown to have a high areal density and in this work we investigate the possibility of improving the uniformity of quantum wires through the use of vicinal (or off-cut) substrates. To our knowledge, the effect of vicinal substrates is still debated since whether it has an effect on the morphology of the grown structure at all seems to depend strongly on the growth conditions. The role of a misoriented surface ranges from being a determining factor of whether wires or dots are grown depending on the off-cut direction [8–10], to improving the size distribution of wires regardless of direction [11] to having very little effect on the nucleation of structures on the substrate surface [12]. However in the research where it has shown an improvement in wire uniformity, the off-cut angle was chosen arbitrarily.

In this work we have grown InAs quantum wires on vicinal substrates with an off-cut angle chosen to match the terrace length to the wire spacing on nominally flat substrates so as to use the steps as nucleation centers similar to observations in [13]. The lateral size distribution of the quantum wires was measured using ultrahigh resolution scanning electron microscopy (SEM) and cross-sectional characterization was performed by high resolution transmission

* Corresponding author.
E-mail address: gbotton@mcmaster.ca (G.A. Botton).

http://dx.doi.org/10.1016/j.jcrysgro.2014.11.028

electron microscopy (HRTEM). Our experimental study was accompanied by kinetic Monte Carlo (kMC) simulations of adatom diffusion including full strain calculations we developed based on work by Schulze and Smereka [14,15] and adapted to the growth of InAs on InGaAlAs. Using our solid on solid cubic model, were able to qualitatively reproduce the quantum wires observed experimentally via the Stranski–Krastanow growth mode and we compared the effects of diffusion anisotropy and bond anisotropy.

2. Materials and methods

2.1. Growth conditions

Eight growth experiments were performed on (001) InP substrates using molecular beam epitaxy (MBE). Half of the substrates were nominally flat ($\pm 0.1^\circ$) and the others were off-cut by 0.9° toward to [110] direction.[1] This angle was chosen such that the length of the atomic steps or atomic terraces (19 nm) should match the spacing of quantum wires grown on flat substrates in previous experiments (see [5] for example). The growth sequence consisted of a 100 nm InP buffer layer to ensure the purity of the substrate before depositing the active layers, a 50 nm InGaAlAs barrier layer lattice-matched to InP, a 5 monolayer[2] (ML) InAs quantum wire layer and another 50 nm InGaAlAs barrier layer for carrier confinement. The first three layers were repeated (InP, InGaAlAs, InAs) in order to produce an exposed surface of quantum wires for SEM characterization.

Each wafer was cleaned using a hydrogen plasma and once heated, the InP buffer layer was grown at 470 °C under a phosphorus overpressure. The quaternary alloy of $In_{.53}Ga_{.47-x}Al_xAs$ was deposited at a rate of 1 ML/s and a temperature of 520 °C for the four first samples, and 535 °C for the other four. The amount of aluminum was $x=0.1$ in one half of the growths and $x=0.2$ in the other. The quantum wires were grown by depositing InAs at a rate of 0.4 ML/s and an As overpressure was applied to maintain a V/III ratio of 4:1 throughout the deposition of the arsenide layers. Cracked arsine and phosphine were used as the group V sources and molten In, Ga and Al were used as the group III sources.

The wires grown on the surface were characterized by scanning electron microscopy (SEM) with an FEI Magellan 400 XHR in secondary electron mode using the through-lens detector and a landing energy between 700 and 1000 eV. Although this technique does not offer a quantitative measurement of the quantum wire height, it allowed us to visually assess their morphology, measure their lateral size distribution and was more convenient than using atomic force microscopy (AFM) for our investigations. In order to measure the spacing distribution of the wires, the micrographs were processed using Fourier bandpass filters, binarized and analyzed using MATLAB.

Cross-sectional wedge samples of the buried wires were prepared and characterized by annular dark field high resolution scanning transmission electron microscopy (ADF-HRSTEM) with an aberration-corrected FEI Titan 80-300. An accelerating voltage of 200 kV was used with a collection angle of 80 mrad. The obtained images were aligned and stitched together using a graphics program to produce a wide-field image with multiple wires so that the off-cut of the substrate and overall off-cut interface can be clearly observed. The atomic dumbbells in the original images were analyzed using principal component analysis (PCA) in order to distinguish the different atomic species in the wire and barrier layer materials

[1] Equivalent to an off-cut toward the [111]A direction.

[2] A monolayer refers to a layer of the group III material which in reality is a III–V bilayer. All materials have a zinc-blende structure.

2.2. Kinetic Monte Carlo model

A kinetic Monte Carlo (kMC) model of adatom diffusion for heteroepitaxy was implemented closely based on one developed by Schulze and Smereka [14,15] and described in detail in Baskaran's thesis [16]. The model is 2+1-dimensional in that it simulates adatoms moving on a 2-dimensional surface or substrate and does not allow the formation of overhangs (solid on solid approximation). Since the growth of III–V semiconductors is limited by the deposition of group III atoms, the diffusion of individual group V atoms is not considered but the effect of the group V overpressure is considered in the bonding strength between neighboring atoms. For simplicity of implementation, rather than a face-centered cubic lattice, the kMC model is based on a tetragonal lattice of the group III atoms where the three orthogonal unit vectors correspond to the (110), $(\bar{1}10)$ and (001) directions of the original crystal. The volume of each unit cell is 1/4 of that of the zinc blende unit cell since each of the latter contains 4 group III atoms.

The simulation uses a rejection-free Monte Carlo method in which the hopping rate R of each adatom is determined by Eq. (1), where R_0 is the base hopping frequency, E_N is the bonding energy between it and neighboring atoms, E_S is the total strain energy contribution of the adatom to the system, E_0 is the activation energy level, k_b is the Boltzmann constant and T is the temperature in K.

$$R = R_0 \exp((E_N + E_S - E_0)/k_b T) \tag{1}$$

The bonding energy considers the first and second nearest neighbors and is modeled based on the surface energy of different facets. The anisotropy of the (2×4) reconstructed zinc blende structure on the (001) surface, which is group V terminated under typical growth conditions [17], is critical to the alignment of InAs quantum wires along the $[\bar{1}10]$ direction. Based on the symmetry of the crystal structure, our model includes 6 distinct bond energies between neighboring atoms (Fig. 1). a_1, a_2 and a_3 are first nearest neighbor bonds while b_1, b_2 and c are second nearest neighbor bonds.

The bond strengths were determined based on the surface energy of crystal facets important to this crystal system. Eqs. (2)–(7) relate the surface energy of 6 facets to the different bonds in our model where γ_{hkl} is the surface energy of the (hkl) facet, l_x, l_y and l_z are the dimensions of our tetragonal unit cell ($l_x = l_y = L/\sqrt{2}$, $l_z = L/2$) and L is the length of the original cubic unit cell. The values of these surface energies for GaAs were taken from density function theory (DFT) calculations by Moll [18] for different surface reconstructions and As chemical potentials which depend on the As overpressure in MBE.

$$\gamma_{001} = \frac{a_3 + 2b_1 + 2b_2}{2l_x l_y} \tag{2}$$

$$\gamma_{100} = \frac{a_1 + a_2 + 2b_1 + 2b_2 + 2c}{2l_z\sqrt{l_x^2 + l_y^2}} \tag{3}$$

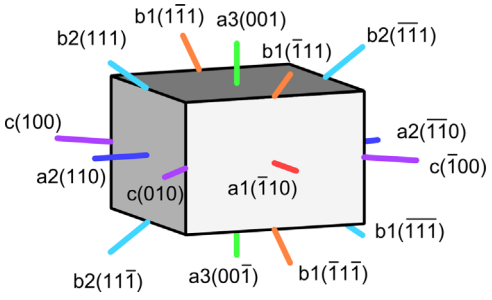

Fig. 1. Different nearest and second nearest neighbor bonds used in our tetragonal unit cell model.

Table 1
The surface energy per surface group III atom in GaAs based on the equilibrium crystal shape (ECS) in [18] and based on our bonding model.

Γ (eV)	ECS	This work
Γ_{001}	1.89	1.86
Γ_{100}	1.89	2.00
$\Gamma_{\bar{1}11}$	2.35	2.38
Γ_{111}	2.12	2.15
$\Gamma_{\bar{1}10}$	1.18	1.07
Γ_{110}	1.18	1.07

$$\gamma_{\bar{1}11} = \frac{a_3 + a_1 + 2b_1 + 2b_2 + 2c}{2l_y\sqrt{l_x^2 + l_z^2}} \tag{4}$$

$$\gamma_{111} = \frac{a_3 + a_2 + 2b_1 + 2b_2 + 2c}{2l_x\sqrt{l_y^2 + l_z^2}} \tag{5}$$

$$\gamma_{\bar{1}10} = \frac{a_1 + 2b_1 + 2c}{2l_y l_z} \tag{6}$$

$$\gamma_{110} = \frac{a_2 + 2b_2 + 2c}{2l_x l_z} \tag{7}$$

The surface energy values were extracted from plots for a chemical potential of $\mu_{As} - \mu_{As(bulk)} = -0.23$ eV (Table 1) and an additional constraint, $(a_1 + a_2)/2 = 4c$, was placed on the bond energies.[3] This choice of surface energies, corresponding to the correct (2×4) reconstruction of the (001) surface, resulted in simulated wires geometrically similar to those observed experimentally and the constraint on c was required to obtain sensible bond strengths which are physically meaningful. The bond energies used in this work were[4]:

$a_1 = 0.382$ eV, $a_2 = 0.153$ eV, $a_3 = 0.537$ eV,
$b_1 = 0.275$ eV, $b_2 = 0.389$ eV, $c = 0.067$ eV.

Based on work done by Grosse and Gyure [19], E_0 was adjusted such that the threshold for Ga to diffuse on a (001) GaAs surface was 1.64 eV, matching their findings. Similar simulations of reflection high-energy electron diffraction (RHEED) oscillations to those done in their work were performed using our model and compared to experimental RHEED oscillation patterns for GaAs in the literature [20] to verify our model's accuracy. These bond and threshold energies (E_N and E_0) obtained for GaAs were then simply scaled by a factor of 0.827 and 1.134 for InAs and AlAs, respectively, based on their relative (110) surface energy in [21]. Since no step bunching was observed in any of our experiments, neither an Ehrlich–Schwoebel barrier [22] nor an incorporation barrier [23] were included.

The strain energy was calculated using a Hookean ball and spring model with two spring constants k_1 and k_2 between first and second nearest neighbors, respectively. In our approximation, their value is given by $k_1 = 4k_2 = 3a_{InP}^3 C_{11}/16$ where a_{InP}^3 is the volume of the substrate's unit cell containing 4 group III atoms and C_{11} is the elastic constant of the material. The strain energy of such Hookean springs is given by $E_S = \frac{1}{2}k\Delta U^2$ where ΔU is the normalized displacement away from equilibrium.[5] The global strain energy of each atom was estimated by evaluating the local strain energy and multiplying it by a factor of 1.3. This factor was determined empirically by comparing the local strain energy around each surface atom in one of our simulations to the total strain energy change in the system when they were removed. A similar factor of 1.33 was used in [15]. Based on elastic constants found in [24–26], the spring constant k_1 for InAs, GaAs and AlAs was 19.7, 28.1 and 28.4 eV. The equilibrium displacement between neighboring "atoms" with respect to the InP substrate was 0.0323, −0.0367 and −0.0354 for InAs, GaAs and AlAs, respectively. Finally, the bond strength, spring constant and equilibrium displacement between two dissimilar materials were taken to be the average, assuming the conditions of an ideal solid solution. We believe this approximation to be valid for our system since experimentally, no significant clustering of different elements was observed in any of the barrier layers beneath the quantum wires and the wires demonstrate strong wetting. This is not the case, however, for InAs quantum wires grown directly on InP which appear far apart [13].

The strain distribution was solved using the successive over-relaxation method. For computational efficiency, after each simulation event the lattice was relaxed locally within a $3\times3\times3$ volume around the displaced atom and every 1000 events, it was relaxed globally using the expanding box method introduced by Schulze and Smereka [14]. Second nearest neighbor springs were actually under-relaxed by a factor of 1/2 in order for the solution to converge.

Additionally, the typical periodic boundary conditions used in most kMC simulations of this kind were adapted in order to simulate a vicinal substrate. Shifted periodic boundary conditions were implemented such that atoms on the right edge of the simulated domain bond to those on the left edge at a different height. Mathematically, this type of periodicity is represented by equation (8) where $f(x,y,z)$ is an arbitrary function of the Cartesian coordinates x, y, z, n_x is the period in x and N_{steps} is the number of steps being simulated. Such boundary conditions allow for the deposition of multiple monolayers onto an off-cut surface but preclude the use the multigrid-Fourier method for solving strain implemented by Russo and Smereka [27].

$$f(x + n_x, y, z) = f(x, y, z - N_{steps}) \tag{8}$$

3. Results and discussion

3.1. SEM characterization

Micrographs of the surface wires grown under different conditions at 520 °C all show densely packed InAs quantum wires with an average spacing of around 20 nm, oriented along the $[\bar{1}10]$ direction (Fig. 2). The wires contain bifurcations, segments which are titled by up to 20° and some quantum dots, all common features to InAs quantum wire growth on arsenide substrates [5]. This differs significantly from wires grown directly on InP where wires are more sparse and their geometry is more strongly affected by the off-cut of the substrate [8]. Although the purpose of growing wires on 0.9° off-cut substrates was to reduce the number of these imperfections and improve the overall size distribution of the quantum wires, there is little, if any visually noticeable improvement between wires grown on the two different surfaces. However, through image analysis, it is possible to distinguish the size distribution of the wires from the different samples.

After applying a bandpass filter and segmenting the SEM micrographs, the separation between the wires was measured throughout each image in order to obtain their horizontal spacing distribution for each sample (Fig. 3). To greatly reduce the dependence of these measurements on the chosen bandpass filter, the distance between the center of adjacent wires is measured instead of the width of the dark region between them. From these results, we can see that the average spacing between the wires grown on $In_{.53}Ga_{.37}Al_{.10}As$ is greater than the spacing between those grown in $In_{.53}Ga_{.27}Al_{.20}As$. This is counterintuitive for the following reason.

[3] The c bond is toward the furthest of the second nearest neighbors.
[4] These bond energies are actually negative.
[5] The normalized displacement is the displacement divided by the lattice constant of the substrate, a_{InP}.

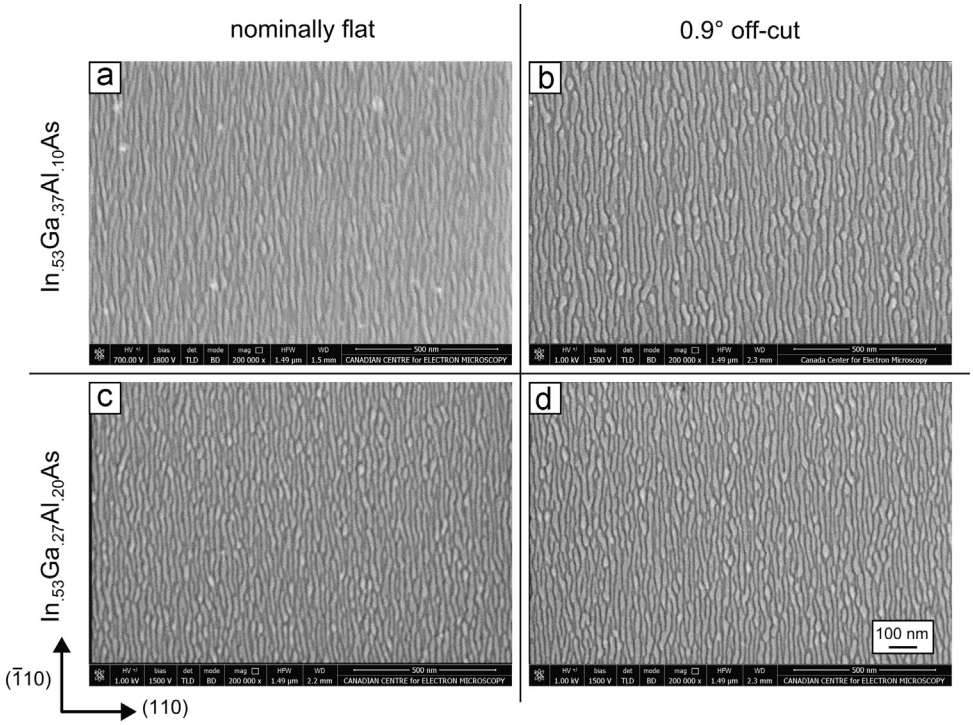

Fig. 2. Secondary electron SEM micrographs showing the topography of InAs quantum wires grown on different substrates under similar conditions (520 °C and 0.4 ML/s.).

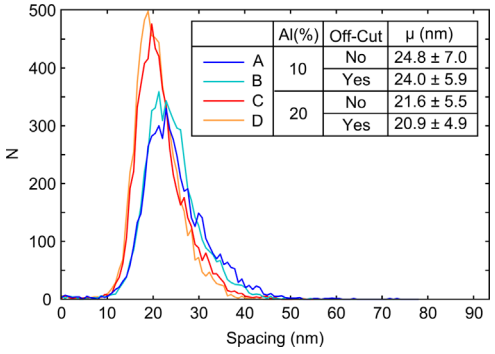

Fig. 3. Spacing distribution of quantum wires in Fig. 2 with the mean spacing and standard deviation (distribution width).

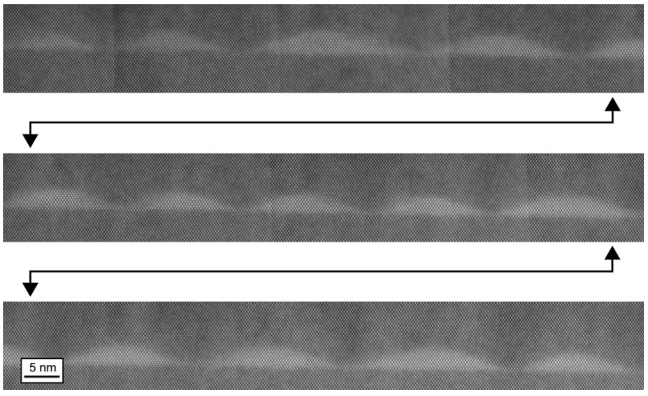

Fig. 4. Cross-sectional HRSTEM image of InAs wires on an off-cut substrate. The stitched images are displayed over three rows and the arrows indicate duplicated regions. The bottom of the image is aligned with a (001) plane, revealing the substrate off-cut.

The width of strain-induced structures depends on the equilibrium between the bonding of the deposited atoms, the stiffness of the material, and the lattice mismatch between the substrate and thin film. Since the strain qualities of AlAs are nearly the same as those of GaAs but Al bonds more strongly than Ga does, we would expect the wires to be wider, not narrower.

With respect to the uniformity of the wire, the width of the spacing distribution was decreased from 7.0 to 5.9 nm on the surface with 10% Al and from 5.5 to 4.9 nm for 20% Al. Based on the collected statistics, the standard deviation of the widths of the distributions was around 0.2 nm meaning that the observed reductions were statistically significant. Despite this, the improvement is modest and our simulation results reveal that this may have been due to the surface being too rough after the deposition of the barrier layer (see Fig. 7).

Additional experiments were performed at 535 °C and resulted in a broad range of morphologies such as quantum wires, quantum dots and exposed regions on the quaternary surface. Based on TEM investigations however, the buried wires appeared to be properly formed. We believe that this deterioration was due to excessive surface migration of the In during the annealing period at the end of the growth which varied from sample to sample. Unlike for the surface wires, the buried wires were covered by the quaternary barrier layer 10 s after being deposited, allowing less time for them to evolve under the high temperature conditions. Given the morphological nature of the wires on the surface, the spacing distribution for these samples would be neither reliable nor relevant.

3.2. TEM characterization

Atomically resolved HRSTEM images taken down the [1̄10] zone axis of a cross-sectional sample grown on an off-cut substrate were aligned and stitched together (Fig. 4). The InAs wires appear brighter since the average atomic number of In (top atomic column of the dumbbells) is greater than that of $In_{.53}Ga_{.37}Al_{.10}$ and the ADF imaging conditions give rise to atomic number contrast.

To compensate for drift and tilting of the sample during the acquisition, the 12 original images were slightly rotated, stretched and skewed to generate a perfect periodic lattice. The required

amount of stretching was less than 5% for all frames. The bottom of the image was aligned to a (001) plane which reveals the off-cut angle of the substrate surface by the decrease in separation between the wire and the bottom of the image from left to right. After analyzing the atomic dumbbells using PCA, it was not possible to determine the position of the atomic steps relative to the wires due to a lack of contrast between the two materials and the strong possibility that the steps were not exactly aligned to the $[\bar{1}10]$ direction (within the thickness of the wedge).

3.3. The effect of anisotropy

Before delving into the simulation of quantum wire growth, we show here the effect that diffusion anisotropy and bond anisotropy have on the shape of islands on a substrate and thus validate our bond model. These terms are defined as they relate to our model. Diffusion anisotropy signifies a global anisotropy of diffusion rates in different directions meaning that atoms are more likely to move along the $[\bar{1}10]$ direction than the [110] direction. Effectively, R_0 from Eq. (1) is split into R_{110} and $R_{\bar{1}10}$. Bond anisotropy denotes different bond energies for neighboring atoms in the $[\bar{1}10]$ (a_1) and [110] (a_2) directions. A subtlety worth noting is that stronger bonds in the $[\bar{1}10]$ direction means that adatoms will move more quickly along steps parallel to the $[\bar{1}10]$ direction than steps perpendicular to it.

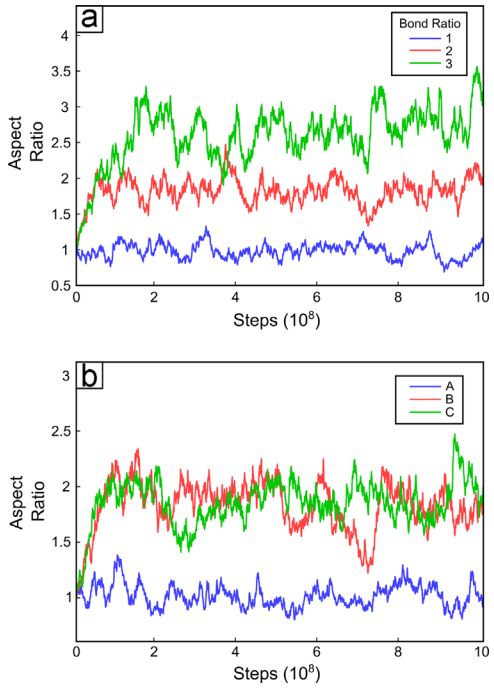

Fig. 5. In (a), the evolution of a 2D island's aspect ratio is shown for bond ratios of 1:1, 2:1 and 3:1. In (b), simulation A had isotropic bonds and a diffusion ratio of 4:1. Simulations B and C had a bond ratio of 2:1 and a diffusion ratio of 4:1 and 1:4, respectively, showing that anisotropic diffusion has no effect on the equilibrium shape of an island.

Simplified simulations with only a_1 and a_2 bonds and without strain were run by starting with a 30 by 30 atom island on a 120 by 120 atom immobile flat substrate and allowing the system to relax under different conditions in terms of bond and diffusion anisotropy. In the first three simulations, the ratio of a_1/a_2 was 1, 2 and 3. Over the course of the simulation, the aspect ratio of the island was obtained by calculating the standard deviation of the position of all the atoms connected to it along the two axes and dividing them (Fig. 5a). In all three cases, the ratio began at 1 and quickly settled to a value near the bond strength ratio among noise due to the stochastic nature of diffusion.

In another set of simulations, namely A, B and C, we illustrate the effect of diffusion anisotropy (Fig. 5b). In A, diffusion was 4 times faster in one direction while the bond strength was isotropic. The aspect ratio of the island was unaffected by this change. Furthermore, simulations B and C were performed with a bond strength ratio of 2:1, and a diffusion ratio of 4:1 and 1:4, respectively. Once again, the aspect ratio of the simulated island quickly reached a value just under 2 and continued to fluctuate about this plateau.

This demonstrates that the shape of islands, at least in equilibrium, depends only on which bond configurations are energetically favorable rather than on any global surface diffusion anisotropy. In fact, given that the bond energies are known, the equilibrium shape can be predicted by counting the number of broken bonds and calculating the surface energy for different island geometries. This is the principle behind the Wulff construction which was of course used to derive Eqs. (2)–(7). Based on such calculations, the expected aspect ratio of islands with our bond model is indeed equal to the ratio of the bond energies as observed.

Moreover, additional growth simulations of quantum wires, not shown here, demonstrated that the ratio of diffusion constants has little to no effect on the morphology of the grown structures which relies on the relative bond strength between neighboring atoms in different crystallographic directions. However, the phenomenon of

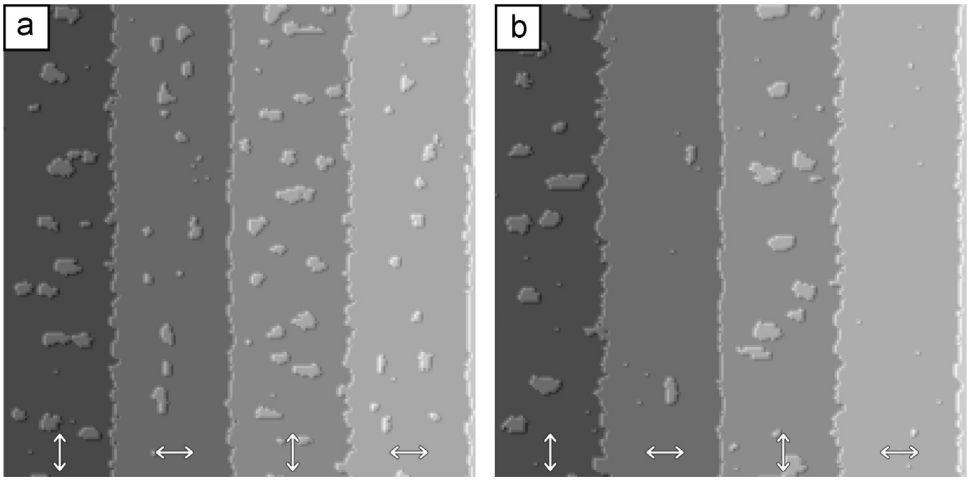

Fig. 6. Alternating anisotropy of islands nucleated on Si terraces due to the inversion of diffusion anisotropy (4:1 ratio). The arrows indicate the direction of faster diffusion. Simulation (b) was carried out at a higher temperature than (a).

alternating smooth and rough edges shown in scanning tunneling microscopy (STM) work by Mo and Lagally [28] was reproducible using our model by alternating the diffusion anisotropy between terraces (Fig. 6). Somewhat counterintuitively, the islands that nucleate on these terraces are longer in the direction opposite to the fast diffusion direction, both in their STM experiment and in our simulations. The dimer rows observed in their experiment however were not reproduced since they rely on the variable attraction between adatoms on the (001) surface, a detail not included in our model. Other more complete models of Si (001) homoeptiaxy already exist [29,30] which simulate phenomena such as step bunching and work by Clarke et al. [31] even shows that bond anisotropy alone provides a better model than diffusion anisotropy alone. Similar conclusions have been drawn elsewhere based on simulations and experiments involving GaAs [32].

Together, this demonstrates that although diffusion anisotropy can play a role in the initial nucleation of islands (or "nuclei"), it does not provide enough of a driving force to produce quantum

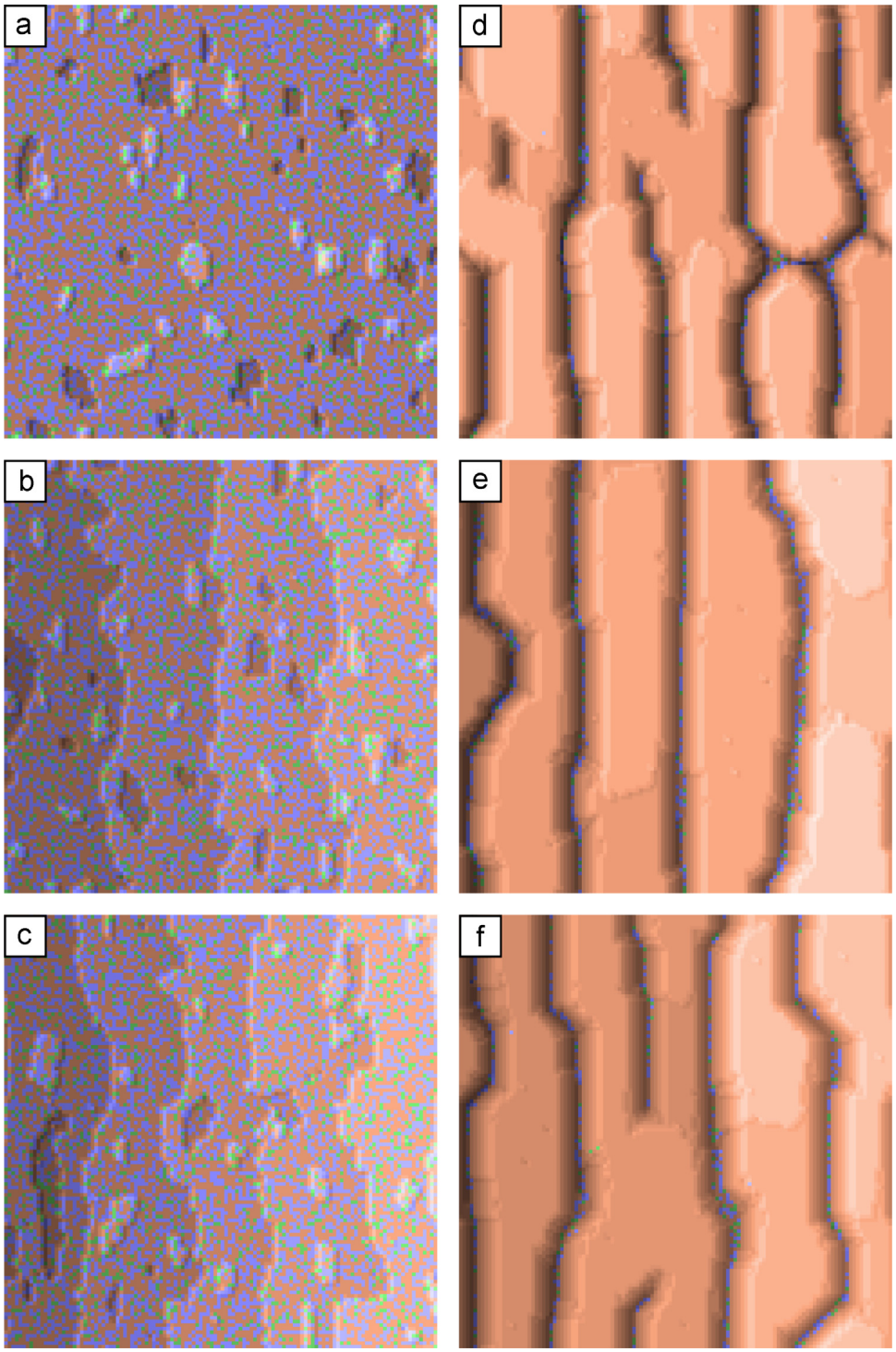

Fig. 7. Simulated growth of quantum wires on flat and off-cut substrates. Figures a, b and c show the $In_{.53}Ga_{.37}Al_{.10}As$ substrate after 10 s of annealing and figures d, e and f show the InAs wires grown on these substrates. From top to bottom there are no steps, 30 atom-wide steps and 24 atom-wide steps. Orange, blue and green pixels represent In, Ga and Al atoms, respectively and their lightness reveals topography. (For interpretation of the references to color in this figure caption, the reader is referred to the web version of this article.)

wires which require a balance between surface energy and strain energy. There is a general consensus that the diffusion of In on the (2×4) As-terminated surfaces present during MBE growth is faster in the $[\bar{1}10]$ direction than in the [110] direction [33,34] but this does not explain the formation of quantum wires as eluded to in some of the literature [35]. If anything, faster diffusion in the $[\bar{1}10]$ direction would lead to the formation of islands in the [110] direction based on our investigations.

Although our model uses anisotropic bonds between neighboring group III atoms to produce a system with the correct surface energies and which forms quantum wires through strain relief, our intention is of course not to imply that this is the physical basis for the phenomenon. To our knowledge the cause is not fully understood but it is likely due to either the energetic favorability of (111)A steps or the As trapping mechanism explained by Grosse whereby only two In atoms are required to bond to an existing island in the $[\bar{1}10]$ direction via an As dimer instead of four in the [110] direction [17]. Such a mechanism is further supported by other kMC models which include As_2 kinetics [36,37]. It is also important to note that this bonding model is only valid for the facets obtainable in our solid on solid model since without considering the group V elements, it is not possible to distinguish the surface energy of (111) and $(\bar{1}\bar{1}\bar{1})$ facets which are different for a zinc blende crystal.

3.4. Quantum wire simulation

The kinetic Monte Carlo model described here was able to produce structures qualitatively similar to experimentally grown InAs quantum wires with many of the same features (Fig. 7). The simulated growth conditions were chosen to match the experimental conditions. 5 ML of $In_{.53}Ga_{.37}Al_{.10}As$ were deposited at a rate of 1 ML/s onto a flat randomly generated substrate of the same quaternary alloy followed by a 10 s "annealing" period where no material was deposited (Fig. 7a–c). The purpose of simulating this layer is not only to produce a realistic surface roughness, but also to hopefully simulate any weak clustering of similar elements that may occur during its formation. Although, clustering is not explicitly considered (ideal solid solution conditions), some grouping of elements may occur due to strain in the same way that the concentration of In is higher directly above the wires in Fig. 4 (brighter contrast) than in regions between the wires. Next, 5 ML of InAs was deposited at a rate of 0.4 ML/s, again followed by a 10 second annealing period (Fig. 7d–f). These growth conditions were repeated on substrates with different step lengths: a substrate with no steps, 30 atom-wide steps and 24 atom-wide steps.

The resulting wires vary in width or spacing, cover the majority of the substrate and have bifurcations as well as rounded ends similar to those in our SEM observations. They appear through the Stranski–Krastanow growth mode whereby a wetting layer first forms on the InGaAlAs substrate and subsequent layers form islands. In this case, as the 3D islands grew, some of the wetting layer material was ejected to compensate for some of the strain produced by the islands. Ga and Al atoms can be seen between the wires. This evolution is distinct from the growth of InAs wires on InP in [13] where wires appear early during growth and are sparsely distributed. The spacing between the wires however is about half of that observed in experiment. This could be attributed to an inaccurate estimate of either the spring constant, the bond strengths or a combination of both, and using a lower spring constant, wires with a spacing near 45 atoms were obtained as in our samples. It is also possible that a tetragonal model for the springs could improve these results. For computational reasons, we continued to use these parameters which provide a convenient number of wires over the simulated area and set the width of the atomic steps accordingly (5 and 4 steps over the area).

The steps clearly have an impact on the resulting wire distribution. The wires in Fig. 7e are more uniform and seem to conform to the shape of the underlying steps. The wires in Fig. 7f are less uniform but still show an improvement over those grown on a flat substrate. This indicates that the choice of the substrate off-cut in terms of matching the wire spacing to the step length is likely an important one. Additionally, the influence of the step shape on that of the wires demonstrates that producing straight steps is important and that the growth conditions of the barrier layer need to be adjusted accordingly. The roughness of the steps in Figs. 7b and 7c show that the deposition rate of 1 ML/s is too high for step-flow growth, especially considering that these simulated steps are narrower than those on the experimental vicinal substrates (24 and 30 atoms vs. 45 atoms). The roughness likely also explains why it was not possible to resolve the position of the atomic steps relative to the quantum wires in our HRSTEM investigation (Fig. 4).

Finally, it is important to mention again that this form of dense quantum wire growth, both simulated and obtained experimentally here, differs significantly from the nucleation of InAs quantum wires grown directly on InP as opposed to on InGaAlAs lattice-matched to InP. Atomic force microscopy (AFM) results in work by Molina [13] reveal the nucleation of quantum wires at surface steps after the deposition of very little In which seems to suggest either strong diffusivity of In on the InP surface during the deposition of InAs (under an As overpressure) or even a repulsion between the arriving In and the unstable group V-terminated substrate as P is being replaced by As. Furthermore, other work [38] attributes the alignment of InAs wires along the $[\bar{1}10]$ direction to an anisotropic stress distribution in the [110] and $[\bar{1}10]$ directions due to the replacement of surface P dimers by As. Although this may be a contributing factor to the formation of InAs wires on InP, there must be some other mechanism present as it is not applicable to quantum wire growth on arsenides.

4. Conclusion

Dense InAs quantum wires were successfully grown on InGaAlAs lattice-matched to InP on both nominally flat and on vicinal substrates with the intent of improving their size distribution. Despite being statistically significant, the improvement in the uniformity of the wires as measured using SEM was small. A kinetic Monte Carlo model of adatom diffusion including strain was developed and used to simulate the formation of InAs quantum wires under similar growth conditions. The results showed that the atomic steps do actually act as nucleation centers for the wires as intended and that under the right growth conditions, we should expect to see an improvement in the uniformity of wires. The simulations also showed that under our experimental conditions, the atomic steps were likely too rough which led to the poor improvement that was observed. The simulated step roughness also explains why no clear location of the atomic steps was observed in our cross-sectional HRSTEM observations. We conclude that in order to produce InAs quantum wires with an improved size distribution, the deposition rate of the InGaAlAs barrier layer should be lowered in order to allow the formation of straight steps under step-flow growth conditions.

Acknowledgments

The authors are grateful to the Natural Sciences and Engineering Research Council (NSERC) for Discovery Grants and to the government of Ontario, Canada for financial support. The microscopy was carried out at the Canadian Centre for Electron Microscopy, a national facility supported by NSERC and McMaster University. A. S. thanks A.

Korinek and M. Bugnet for assistance with microscopy and S. Tavakoli with MBE.

References

[1] Z. Mi, P. Bhattacharya, Molecular-beam epitaxial growth and characteristics of highly uniform InAsGaAs quantum dot layers, J. Appl. Phys. 98 (2) (2005) 023510. http://dx.doi.org/10.1063/1.1985969.

[2] D. Wohlert, S. Chou, K. Cheng, Temperature-insensitive photoluminescence above 300 K in strained GaxIn1 x As multiple quantum wire heterostructures, J. Cryst. Growth 175–176 (1997) 1162–1166. http://dx.doi.org/10.1016/S0022-0248(96)01032-9.

[3] T. Miya, Y. Terunuma, T. Hosaka, T. Miyashita, Ultimate low-loss single-mode fibre at 1.55 μm, Electron. Lett. 15 (4) (1979) 106. http://dx.doi.org/10.1049/el:19790077.

[4] F. Suárez, D. Fuster, L. Gonzalez, Self-assembled InAs quantum wire lasers on (001) InP at 1.6 μm, Appl. Phys. 091123 (001) (2006) 2004–2007. http://dx.doi.org/10.1063/1.2335775.

[5] K. Cui, B.J. Robinson, D.a. Thompson, G.a. Botton, Effect of layer separation, InAs thickness, and rapid thermal annealing on the optical emission from a multi-layer quantum wire structure, J. Appl. Phys. 109 (12) (2011) 124311. http://dx.doi.org/10.1063/1.3598082.

[6] T. Amano, T. Sugaya, K. Komori, 1.3-/spl mu/m InAs quantum-dot laser with high dot density and high uniformity, Photon. Technol. Lett. 18 (4) (2006) 619–621, URL: ⟨http://ieeexplore.ieee.org/xpls/abs_all.jsp?arnumber=1588983⟩.

[7] J.S. Kim, J.H. Lee, S.U. Hong, W.S. Han, H.-S. Kwack, C.W. Lee, D.K. Oh, J. Cryst. Growth 259 (3) (2003) 252–256. http://dx.doi.org/10.1016/j.jcrysgro.2003.07.018, URL: ⟨http://linkinghub.elsevier.com/retrieve/pii/S0022024803016580⟩.

[8] O. Bierwagen, W.T. Masselink, Self-organized growth of InAs quantum wires and dots on InP(001): the role of vicinal substrates, Appl. Phys. Lett. 86 (11) (2005) 113110. http://dx.doi.org/10.1063/1.1884762, URL: ⟨http://link.aip.org/link/APPLAB/v86/i11/p113110/s1&Agg=doi.

[9] B. Salem, J. Olivares, G. Guillot, G. Bremond, J. Brault, C. Monat, M. Gendry, G. Hollinger, F. Hassen, H. Maaref, Optical properties of self-assembled InAs quantum islands grown on InP(001) vicinal substrates, Appl. Phys. Lett. 79 (26) (2001) 4435. http://dx.doi.org/10.1063/1.1427742, URL: ⟨http://link.aip.org/link/APPLAB/v79/i26/p4435/s1&Agg=doi⟩.

[10] G. Elias, A. Letoublon, R. Piron, I. Alghraibi, K. Tavernier, N. Chevalier, N. Bertru, A. Le Corre, S. Loualiche, Improvement of 1.55 μm InAs QD laser using vicinal (001)InP substrate, in: IPRM '09. IEEE International Conference on Indium Phosphide Related Materials, 2009, pp. 41–44. http://dx.doi.org/10.1109/ICIPRM.2009.5012422.

[11] W. Lei, Y.L. Wang, Y.H. Chen, P. Jin, X.L. Ye, B. Xu, Z.G. Wang, Effect of substrate misorientation on the InAsInAlAsInP nanostructure morphology and lateral composition modulation in the InAlAs matrix, Appl. Phys. Lett. 90 (10) (2007) 103118. http://dx.doi.org/10.1063/1.2711778, URL: ⟨http://link.aip.org/link/APPLAB/v90/i10/p103118/s1&Agg=doi⟩.

[12] N. Sritirawisarn, F.W.M. van Otten, T.J. Eijkemans, R. Notzel, Formation of linear InAs quantum dot arrays on InGaAsPInP (100) by self-organized anisotropic strain engineering and their optical properties, J. Appl. Phys. 102 (5) (2007) 053514. http://dx.doi.org/10.1063/1.2777198, URL: ⟨http://scitation.aip.org/content/aip/journal/jap/102/5/10.1063/1.2777198⟩.

[13] S.I. Molina, M. Varela, D.L. Sales, T. Ben, J. Pizarro, P.L. Galindo, D. Fuster, Y. Gonzalez, L. Gonzalez, S.J. Pennycook, Direct imaging of quantum wires nucleated at diatomic steps, Appl. Phys. Lett. 91 (14) (2007) 143112. http://dx.doi.org/10.1063/1.2790483, URL: ⟨http://link.aip.org/link/APPLAB/v91/i14/p143112/s1&Agg=doi⟩.

[14] T.P. Schulze, P. Smereka, An energy localization principle and its application to fast kinetic Monte Carlo simulation of heteroepitaxial growth, J. Mech. Phys. Solids 57 (3) (2009) 521–538. http://dx.doi.org/10.1016/j.jmps.2008.11.007, URL: ⟨http://linkinghub.elsevier.com/retrieve/pii/S002250960800197X⟩.

[15] T.P. Schulze, P. Smereka, Kinetic Monte Carlo simulation of heteroepitaxial growth: wetting layers, quantum dots, capping, and nanorings, Phys. Rev. B 86 (23) (2012) 235313. http://dx.doi.org/10.1103/PhysRevB.86.235313, URL: ⟨http://link.aps.org/doi/10.1103/PhysRevB.86.235313⟩.

[16] A. Baskaran, Modeling and simulation of heteroepitaxial growth (Ph.D. thesis), University of Michigan, 2009. URL: ⟨http://141.213.232.243/handle/2027.42/63846⟩.

[17] F. Grosse, M. Gyure, Island and step morphology in InAs(001) homoepitaxy, Phys. Status Solidi (B) 234 (1) (2002) 338–345 http://dx.doi.org/10.1002/1521-3951(200211)234:1 < 338::AID-PSSB338 > 3.0.CO;2-F URL: ⟨http://doi.wiley.com/10.1002/1521-3951(200211)234:1 < 338::AID-PSSB338 > 3.0.CO;2-F.

[18] N. Moll, a. Kley, E. Pehlke, M. Scheffler, GaAs equilibrium crystal shape from first principles, Phys. Rev. B Condens. Matter 54 (12) (1996) 8844–8855, URL: ⟨http://www.ncbi.nlm.nih.gov/pubmed/9984566⟩.

[19] F. Grosse, R. Zimmermann, Monte Carlo growth simulation for AlxGa1xAs heteroepitaxy, J. Cryst. Growth 212 (1–2) (2000) 128–137. http://dx.doi.org/10.1016/S0022-0248(99)00848-9, URL: ⟨http://linkinghub.elsevier.com/retrieve/pii/S0022024899008489⟩.

[20] J. Neave, P. Dobson, Reflection high-energy electron diffraction oscillations from vicinal surfaces a new approach to surface diffusion measurements, Appl. Phys. 100 (1985) 1–4. http://dx.doi.org/10.1063/1.96281, URL: ⟨http://ieeexplore.ieee.org/xpls/abs_all.jsp?arnumber=4854112⟩.

[21] W. Liu, W. Zheng, Q. Jiang, First-principles study of the surface energy and work function of III–V semiconductor compounds, Phys. Rev. B 75 (23) (2007) 235322. http://dx.doi.org/10.1103/PhysRevB.75.235322, URL: ⟨http://link.aps.org/doi/10.1103/PhysRevB.75.235322⟩.

[22] R.L. Schwoebel, Step motion on crystal surfaces. II, J. Appl. Phys. 40 (2) (1969) 614. http://dx.doi.org/10.1063/1.1657442, URL: ⟨http://scitation.aip.org/content/aip/journal/jap/40/2/10.1063/1.1657442⟩.

[23] M. Xie, S. Leung, S. Tong, What causes step bunching negative Ehrlich Schwoebel barrier versus positive incorporation barrier, Surf. Sci. 515 (1) (2002) L459–L463. http://dx.doi.org/10.1016/S0039-6028(02)01976-3, URL: ⟨http://linkinghub.elsevier.com/retrieve/pii/S0039602802019763⟩.

[24] NSM Archive—Physical Properties of Semiconductors (2013). URL: ⟨http://www.ioffe.ru/SVA/NSM/Semicond/index.html⟩.

[25] S. Adachi, GaAs, AlAs, and AlxGa1xAs material parameters for use in research and device applications, J. Appl. Phys. 58 (3) (1985) R1. http://dx.doi.org/10.1063/1.336070, URL: ⟨http://scitation.aip.org/content/aip/journal/jap/58/3/10.1063/1.336070⟩.

[26] Y.A. Burenkov, S.Y. Davydov, S. Nikanorov, The elastic properties of indium arsenide, Sov. Phys. Solid State 17 (7) (1975) 1446–1447.

[27] G. Russo, P. Smereka, A multigrid-Fourier method for the computation of elastic fields with application to heteroepitaxy, Multiscale Model. Simul. 5 (1) (2006) 130–148. http://dx.doi.org/10.1137/05063800X, URL: ⟨http://epubs.siam.org/doi/abs/10.1137/05063800X⟩.

[28] Y. Mo, M. Lagally, Anisotropy in surface migration of Si and Ge on Si(001), Surf. Sci. 248 (3) (1991) 313–320. http://dx.doi.org/10.1016/0039-6028(91)91177-Y, URL: ⟨http://www.sciencedirect.com/science/article/pii/003960289191177Yhttp://linkinghub.elsevier.com/retrieve/pii/003960289191177Y⟩.

[29] J. Mysliveček, C. Schelling, G. Springholz, F. Schäffler, B. Voigtländer, P. Šmilauer, On the origin of the kinetic growth instability of homoepitaxy on Si(001), Mater. Sci. Eng. B 89 (1–3) (2002) 410–414. http://dx.doi.org/10.1016/S0921-5107(01)00844-3, URL: ⟨http://linkinghub.elsevier.com/retrieve/pii/S0921510701008443⟩.

[30] B. Voigtländer, T. Weber, P. Šmilauer, D. Wolf, Transition from island growth to step-flow growth for Si/Si(100) epitaxy, Phys. Rev. Lett. 78 (11) (1997) 2164–-2167. http://dx.doi.org/10.1103/PhysRevLett.78.2164, URL: ⟨http://link.aps.org/doi/10.1103/PhysRevLett.78.2164⟩.

[31] S. Clarke, M. Wilby, D. Vvedensky, Theory of homoepitaxy on Si(001), Surf. Sci. 255 (1–2) (1991) 91–110. http://dx.doi.org/10.1016/0039-6028(91)90013-I, URL: ⟨http://linkinghub.elsevier.com/retrieve/pii/003960289190013I⟩.

[32] T. Shitara, D. Vvedensky, M. Wilby, Step-density variations and reflection high-energy electron-diffraction intensity oscillations during epitaxial growth on vicinal GaAs (001), Phys. Rev. B 46 (11) (1992) 6815–6824, URL: ⟨http://journals.aps.org/prb/abstract/10.1103/PhysRevB.46.6815⟩.

[33] L. Huang, F. Liu, X. Gong, Strain effect on adatom binding and diffusion in homo- and heteroepitaxies of Si and Ge on (001) surfaces, Phys. Rev. B 70 (15) (2004) 1–6. http://dx.doi.org/10.1103/PhysRevB.70.155320, URL: ⟨http://link.aps.org/doi/10.1103/PhysRevB.70.155320⟩.

[34] K. Ohta, T. Kojima, T. Nakagawa, Anisotropic surface migration of Ga atoms on GaAs (001), J. Cryst. Growth 95 (1–4) (1989) 71–74. http://dx.doi.org/10.1016/0022-0248(89)90354-0, URL: ⟨http://linkinghub.elsevier.com/retrieve/pii/0022024889903540⟩.

[35] J. Brault, M. Gendry, G. Grenet, G. Hollinger, Y. Desieres, T. Benyattou, Role of buffer surface morphology and alloying effects on the properties of InAs nanostructures grown on InP(001), Appl. Phys. Lett. 73 (20) (1998) 2932. http://dx.doi.org/10.1063/1.122634, URL: ⟨http://scitation.aip.org/content/aip/journal/apl/73/20/10.1063/1.122634⟩.

[36] P. Kratzer, M. Scheffler, Reaction-limited island nucleation in molecular beam epitaxy of compound semiconductors, Phys. Rev. Lett. 88 (3) (2002) 036102. http://dx.doi.org/10.1103/PhysRevLett.88.036102, URL: ⟨http://link.aps.org/doi/10.1103/PhysRevLett.88.036102⟩.

[37] M. Itoh, G. Bell, A. Avery, T. Jones, B. Joyce, D. Vvedensky, Island nucleation and growth on reconstructed GaAs(001) surfaces, Phys. Rev. Lett. 81 (3) (1998) 633–636. http://dx.doi.org/10.1103/PhysRevLett.81.633, URL: ⟨http://link.aps.org/doi/10.1103/PhysRevLett.81.633⟩.

[38] J. Garca, L. González, M. González, J. Silveira, Y. González, F. Briones, InAs/InP (001) quantum wire formation due to anisotropic stress relaxation: in situ stress measurements, J. Cryst. Growth 227–228 (2001) 975–979. http://dx.doi.org/10.1016/S0022-0248(01)00962-9, URL: ⟨http://www.sciencedirect.com/science/article/pii/S0022024801009629http://linkinghub.elsevier.com/retrieve/pii/S0022024801009629⟩.